Making Topologically Trivial Non-Hermitian Systems Nontrivial via Gauge Fields

W. B. Rui,* Y. X. Zhao,† and Z. D. Wang‡
Department of Physics and HK Institute of Quantum Science & Technology, The University of Hong Kong, Pokfulam Road, Hong Kong, China

(Received 2 December 2022; revised 15 February 2023; accepted 22 September 2023; published 25 October 2023)

Non-Hermiticity significantly enriches the concepts of symmetry and topology in physics. Particularly, non-Hermiticity gives rise to the ramified symmetries, where the non-Hermitian Hamiltonian H is transformed to $H^\dagger$. For time-reversal (T) and sublattice symmetries, there are six ramified symmetry classes leading to novel topological classifications with various non-Hermitian skin effects. As artificial crystals are the main experimental platforms for non-Hermitian physics, there exists the symmetry barrier for realizing topological physics in the six ramified symmetry classes: while artificial crystals are in spinless classes with $T^2 = 1$, nontrivial classifications dominantly appear in spinful classes with $T^2 = -1$. Here, we present a general mechanism to cross the symmetry barrier. With an internal parity symmetry P, the square of the combination $\tilde{T} = PT$ can be modified by appropriate gauge fluxes. Using the general mechanism, we systematically construct spinless models for all non-Hermitian spinful topological phases in one and two dimensions, which are experimentally realizable. Our Letter suggests that gauge structures may significantly enrich non-Hermitian physics at the fundamental level.

DOI: 10.1103/PhysRevLett.131.176402

Introduction.—Recently, non-Hermitian topology has attracted great interest [1–20], ranging from fundamental concepts to fascinating phenomena such as complex-energy gaps [21,22], non-Bloch band theory [23–26], exceptional degeneracies [27–32], and non-Hermitian skin effects [23,33–37]. Analogous to the Hermitian topology, symmetry remains to be foundational for non-Hermitian topology, as it provides the framework for topological classifications [22,38]. But for a non-Hermitian Hamiltonian H, the Hermitian conjugate $H^\dagger$ is not equal to H. This gives rise to a new possibility for symmetry. A symmetry may transform H to $H^\dagger$, rather than leave H invariant. Such a symmetry is referred to as ramified symmetry [22,38–40]. As a prominent example, the ten Altland-Zirnbauer (AZ) symmetry classes have been extended into 38 symmetry classes with eight additional ramified AZ† symmetry classes [41]. Topological classifications have been worked out for the ramified symmetry classes; nontrivial topology can lead to the non-Hermitian skin effect, featuring the breakdown of conventional bulk-boundary correspondence.

Here, among the eight ramified AZ† symmetry classes, we focus on the six ones with time-reversal (T) symmetry. Note that the other two contain particle-hole symmetry for superconductors, and therefore are not considered here. We further categorize the six classes with T symmetry into three spinless and three spinful classes with $T^2 = 1$ and $T^2 = -1$, respectively. The topological classification table for point-gap systems [42] in one and two dimensions is given by Fig. 1(a) [43], as the skin effect is mainly investigated in the low dimensions. From Fig. 1(a), it is exciting to observe various nontrivial topological classifications, which dominantly belong to the spinful classes. The situation is unfortunate for experimental realization because non-Hermitian topology is mainly realized by artificial crystals, e.g., photonic and acoustic crystals and electric-circuit arrays. All these artificial crystals satisfy $T^2 = 1$, and therefore belong to spinless classes. Hence, we see that there is the symmetry barrier preventing broad realizations of non-Hermitian topological phases by artificial crystals.

In this Letter, we provide general mechanisms by which the symmetry barrier can be crossed. The key observation is that for 1D and 2D systems, we can consider two antiunitary symmetries, T and $\tilde{T} = PT$, with P a twofold internal symmetry. For both 1D and 2D systems, P can be the mirror reflection M_z inversing the z axis, presuming that the system is placed on the x-y plane. For a 1D system, we may choose P as the twofold rotation C through the direction of the 1D system.

Ordinarily, $\tilde{T}^2 = T^2$, but by turning on in-plane or in-line gauge fluxes, we may have

$$\tilde{T}^2 = -T^2. \tag{1}$$

Here, the font is changed with gauge fluxes, noting that the intrinsic T cannot be changed by gauge fluxes. This is because the symmetry group is projectively represented in the presence of gauge fluxes, i.e., gauge fluxes can induce additional phase factors into the symmetry multiplications, resembling the Aharonov-Bohm effect. Particularly, for

(a)

	T^2	S	$d=1$	$d=2$
AI†	$+$	0	0	0
BDI†	$+$	$[S,T]=0$	0	0
CI†	$+$	$\{S,T\}=0$	0	$2\mathbb{Z}$

gauge ⇓ field

	$\tilde{\mathcal{T}}^2$	S	$d=1$	$d=2$
AII†	$-$	0	$\mathbb{Z}_2$	$\mathbb{Z}_2$
CII†	$-$	$[S,\tilde{\mathcal{T}}]=0$	0	$\mathbb{Z}_2$
DIII†	$-$	$\{S,\tilde{\mathcal{T}}\}=0$	$\mathbb{Z}_2$	$\mathbb{Z}$

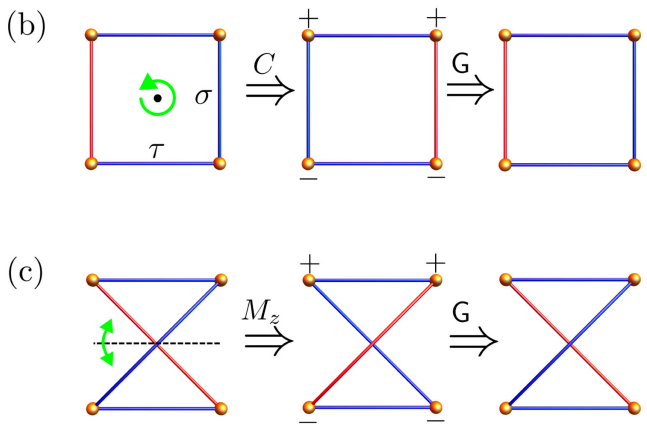

FIG. 1. (a) Classification of spinless (upper table) and spinful (lower table) classes with ramified time-reversal and sublattice symmetries for point-gap topological phases [22,42]. See Ref. [43] for the connection of our convention to the previous convention of the symmetry classes. The symmetry barrier between spinless and spinful classes can be crossed by gauge field. (b) Rectangle with π gauge flux, invariant under the projective twofold rotation. (c) Twisted rectangle with π gauge flux, invariant under the projective mirror reflection. Blue and red denote the $+$ and $-$ hopping amplitudes, respectively. The gauge transformations (G) are specified by the signs in the two middle panels.

$P=C$ or M_z the additional minus sign in (1) shall be realized with appropriate gauge fluxes. Then, for spinless systems, we can realize $\tilde{\mathcal{T}}^2=-T^2=-1$ according to (1). Thus, $\tilde{\mathcal{T}}$ becomes the fundamental symmetry for us. To realize spinful non-Hermitian topologies by spinless systems, we can preserve $\tilde{\mathcal{T}}$ while allowing T to be broken. This is illustrated in Fig. 2(b); with the insertion of gauge fluxes, the spinful skin states rise on a previously trivial spinless chain.

We thoroughly implement the mechanism for all nontrivial cases in the classification table of Fig. 1(a). That is, we systematically construct spinless models that can realize all spinful non-Hermitian topological phases. All the spinless models for spinful non-Hermitian topological phases can be realized by artificial crystals. For demonstration, we explicitly design the electric-circuit realization of a representative phase. Besides the immediate experimental interest, our Letter evidences that modulating gauge degrees of freedom may lead to unprecedented mechanisms and phenomena in non-Hermitian physics, which is a promising direction to explore.

Breaking symmetry restrictions by $\mathbb{Z}_2$ gauge fields.—The modification of symmetry algebras with additional phase factors resembles the Aharonov-Bohm effect. Hence, to facilitate the minus sign in (1), it is sufficient to consider π fluxes with gauge connections valued in $\mathbb{Z}_2=\{\pm1\}$, i.e., each hopping amplitude takes phases 0 or π and therefore is a positive or negative real number.

Then, for a plaquette with flux π, there are odd negative ones among the hopping amplitudes surrounding it. However, as illustrated in Figs. 1(b) and 1(c), although the π-flux preserves $P=C$ or M_z, the gauge-connection configuration A does not in general. P transforms it to another configuration A' that equally describes the π-flux configuration. Hence, the two gauge-connection configurations A and A' are related by a gauge transformation G, i.e., to restore the original A, a gauge transformation G should be imposed. Then, the parity operator that operates on the Hamiltonian should be the combination

$$\mathcal{P}=\mathsf{G}P. \tag{2}$$

Since $[T,\mathsf{G}]=[T,P]=0$, to realize (1) we require $\mathcal{P}^2=-1$. This in turn requires the anticommutation relation $\{\mathsf{G},P\}=0$, noting that $P^2=\mathsf{G}^2=1$. It is noteworthy that G is just a diagonal matrix with diagonal entries ±1, where the matrix indexes are just the lattice sites. Thus, G can be visualized on the lattice by assigning each lattice site the corresponding sign (see Fig. 1). Then, $\{\mathsf{G},P\}=0$ implies P reverses the signs of all lattice sites.

Particularly, let us consider the lattice blocks for $P=C$ and M_z, respectively, illustrated in Figs. 1(b) and 1(c). For $P=C$ illustrated in Fig. 1(b), we see that $C=\tau_1\otimes\sigma_1$ and $\mathsf{G}=\tau_3\otimes\sigma_0$, and clearly C reverses signs of G. Here, τ and σ are two sets of the standard Pauli matrices operating on the row and column indexes, respectively. Hence, $\{C,\mathsf{G}\}=0$, and

$$\mathcal{C}=\mathsf{G}C=i\tau_2\otimes\sigma_1 \tag{3}$$

with $\mathcal{C}^2=-1$. For the mirror reflection, namely $P=M_z$, the operators are read off from Fig. 1(c) as $\mathsf{G}=\tau_3\otimes\sigma_0$ and $M_z=\tau_1\otimes\sigma_0$. Accordingly, we have

$$\mathcal{M}_z=i\tau_2\otimes\sigma_0 \tag{4}$$

with $\mathcal{M}_z^2=-1$.

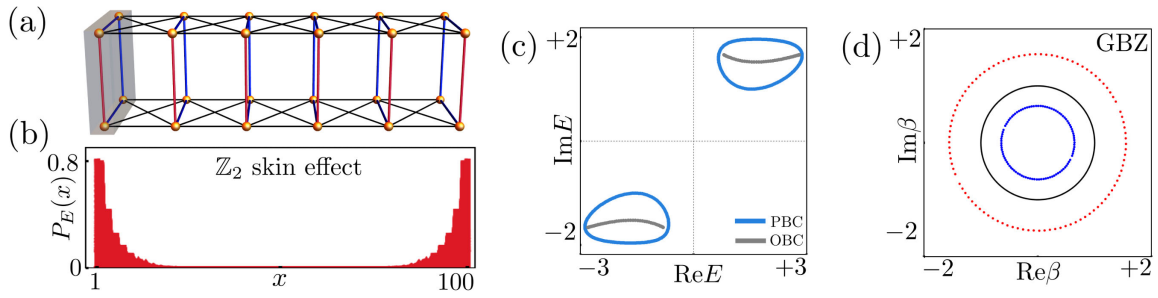

FIG. 2. (a) Schematic picture for the 1D spinless chain. The unit cell is constructed by the rectangle in Fig. 1(b), which is marked by gray. (b) The $\mathbb{Z}_2$ non-Hermitian skin effect. For the Hamiltonian with 100 unit cells under the open boundary conditions, we compute all the energy eigenstates $|\psi_E\rangle$ with energy E. For each E, we plot $P_E(x) = \sum_\alpha |\langle x, \alpha|\psi_E\rangle|^2$, where $|x, \alpha\rangle$ is the on-site state at αth site in the xth unit cell. (c) The energy spectra and (d) the generalized Brillouin zone (blue and red) of the system. The black circle in (d) denotes $|\beta| = 1$. The parameters are $J_R = J_I = 1.5$, $t = \mu = 1$, $\gamma = 2$.

Then, the gauge-field enriched time-reversal symmetry is given by $\tilde{\mathcal{T}} = \mathcal{P}T$ with $\mathcal{P} = \mathcal{C}$ or $\mathcal{M}_z$. In momentum space, $T = U_T K I$ with I the inversion of momenta and K the complex conjugation. The non-Hermitian Hamiltonian $\mathcal{H}(\boldsymbol{k})$ in the ramified symmetry classes is constrained by $\tilde{\mathcal{T}} = \tilde{U}_T K I$ as

$$\tilde{U}_T \mathcal{H}(\boldsymbol{k})^* \tilde{U}_T^\dagger = \mathcal{H}(-\boldsymbol{k})^\dagger. \tag{5}$$

Here, $\tilde{U}_T = \mathcal{P}U_T$. In addition to the ramified time reversal, we also consider the ramified sublattice symmetry $\mathcal{S}$, which exerts the following constraint on the Hamiltonian:

$$\mathcal{S}\mathcal{H}^\dagger(\boldsymbol{k})\mathcal{S} = -\mathcal{H}(\boldsymbol{k}). \tag{6}$$

Here, $\mathcal{S}$ is a unitary operator with $\mathcal{S}^2 = 1$. Hence, $\mathcal{S}$ is Hermitian unitary with $\mathcal{S}^\dagger = \mathcal{S}$.

1D spinful non-Hermitian topological phase and $\mathbb{Z}_2$ skin effect in spinless chains.—Let us first consider 1D systems. According to the classification table of Fig. 1(a), the emergence of any nontrivial topological phase is forbidden in 1D spinless systems with $T^2 = +1$. Thus, it was previously concluded that the non-Hermitian skin effect, which manifests as the non-Hermitian bulk-boundary correspondence, is not allowed in these systems [44,45]. On the contrary, nontrivial spinful topology is permitted in 1D. Here, we show that nontrivial topology in both of the two 1D spinful classes (AII† and DIII†) in Fig. 1(a) can be constructed using the rectangle with π flux of Fig. 1(b).

We focus on the topological phase in AII† class, which possesses a spinful $\mathbb{Z}_2$ non-Hermitian skin effect, and leave the DIII† class in the Supplemental Material (SM) [46]. We can build the 1D lattice model as shown in Fig. 2(a). The momentum-space Hamiltonian reads,

$$\begin{aligned}\mathcal{H}(k) = {} & J_R \tau_0 \otimes \sigma_1 - J_I \tau_1 \otimes \sigma_3 + t \cos k \tau_0 \otimes \sigma_1 \\ & + t \sin k \tau_0 \otimes \sigma_3 + \mu \tau_0 \otimes \sigma_2 + i\gamma \tau_0 \otimes \sigma_1,\end{aligned} \tag{7}$$

where J_R and J_I are hoppings inside unit cells, t denotes the hopping between unit cells, μ is a constant potential, and $i\gamma\tau_0 \otimes \sigma_1$ is responsible for non-Hermiticity. We plot the energy spectra of the system under open boundary condition (OBC) and periodic boundary condition (PBC) in Fig. 2(c).

Figure 2(b) shows the wave function profile of the system under OBC. Evidently, a spinful $\mathbb{Z}_2$ non-Hermitian skin effect emerges in this spinless chain, indicating the breakdown of symmetry restrictions on this 1D spinless system. As previously explained, this is achieved by the gauge-field enriched time-reversal symmetry in Eq. (5) as

$$\tilde{\mathcal{T}} = \mathcal{C}T = i\tau_2 \otimes \sigma_1 K I, \qquad \tilde{\mathcal{T}}^2 = -1, \tag{8}$$

which leads to a $\mathbb{Z}_2$ topological invariant $\nu(E) \in \{0, 1\}$ in 1D [33],

$$\begin{aligned}(-1)^{\nu(E)} = \operatorname{sgn}\Bigg\{ & \frac{Pf[(\mathcal{H}(\pi) - E)\tilde{U}_T]}{Pf[(\mathcal{H}(0) - E)\tilde{U}_T]} \\ & \times \exp\left(-\frac{1}{2}\int_{k=0}^{k=\pi} d \log \det[(\mathcal{H}(k) - E)\tilde{U}_T]\right)\Bigg\}.\end{aligned} \tag{9}$$

Here, $\tilde{U}_T = i\tau_2 \otimes \sigma_1$, Pf denotes the Pfaffian of skew symmetric matrices [50], and E is a reference energy. We find the nontrivial $\nu(E) = 1$ for E inside the closed curve of PBC spectrum. This topological invariant dictates the emergence of $\mathbb{Z}_2$ non-Hermitian skin effect localized at both ends of the OBC systems as shown in Fig. 2(b).

The spinful $\mathbb{Z}_2$ skin effect can be understood by using the generalized Brillouin zone (GBZ) [23–25], which is a generalization of the Bloch Hamiltonian by the substitution of $e^{ik} \to \beta$ in $\mathcal{H}(k)$ to describe non-Hermitian OBC systems. The non-Hermitian skin effect emerges when $|\beta| \neq |e^{ik}| = 1$. Note that skin modes with $|\beta| > 1$ and those with $|\beta| < 1$ are localized at opposite ends. Under the

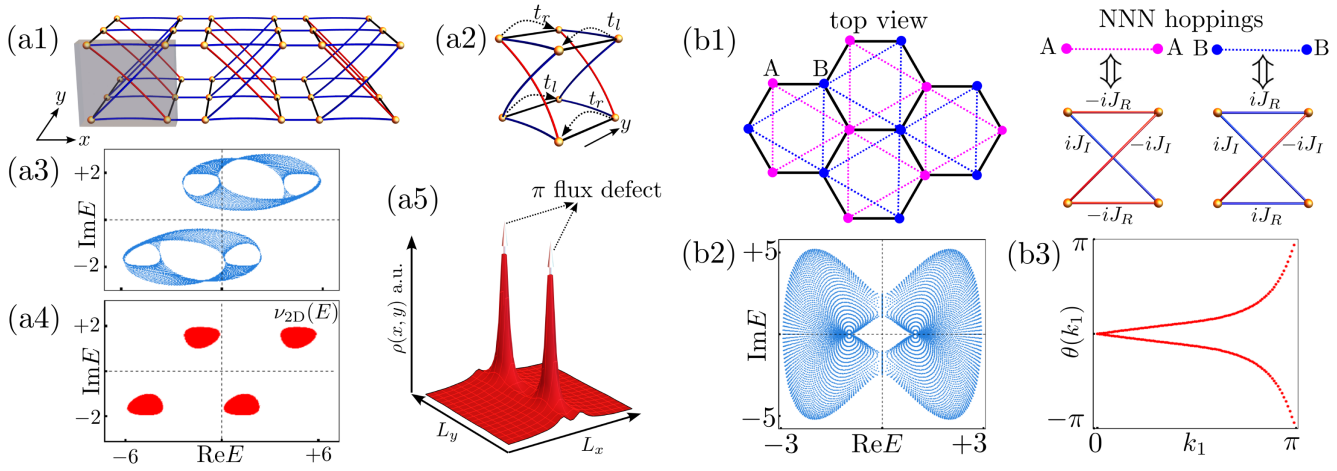

FIG. 3. (a1) Schematic picture for the 2D lattice in AII† class. The unit cell marked in gray. (a2) The nonreciprocal hoppings in the y direction. (a3) The PBC spectrum, and (a4) the topological invariant of the system. (a5) The non-Hermitian flux skin effect, which is localized at the cores of the π flux defects. At the (x, y) position, the density is $\rho(x, y) = \sum_{\alpha,\beta} |\langle x, y, \alpha|\psi_\beta\rangle|^2$, where α runs over all internal degrees of unit cell and β all eigenstates. Full PBC is taken to avoid boundary effects. The parameters are $J_R = J_I = 1.5$, $\gamma = t_r = 2$, $t = t_l = 1$. (b1) Schematic picture for the bilayer hexagonal lattice. The two layers are connected by lattice blocks adjusted from Fig. 1(c), as shown in the right. (b2) The PBC spectrum of the system, and (b3) the Wilson loop spectrum. The parameters are $t = J_I = 1$, $J_R = 0.1$.

spinful time-reversal symmetry of Eq. (8), the skin mode $|\beta, +\rangle$ is mapped to $|1/\beta, -\rangle$ in a Kramers pair [26,44]. Here, $\pm$ denotes the two pseudospin states. The GBZ for symmetry-related pseudospin bands is shown by red and blue curves in Fig. 2(d), which have inverse β to each other. Thus, the spinful $\mathbb{Z}_2$ non-Hermitian skin effect is formed by the Kramers pairs of skin modes localized at opposite ends.

2D non-Hermitian spinful topological phases and flux skin effect in spinless lattices.—We proceed to discuss the realization of 2D spinful topological phases in spinless lattices. Among the three nontrivial 2D spinful classes in the lower table of Fig. 1(a), we discuss two classes of AII† and CII† in the following, and leave DIII† class in the SM [46]. Notably, for AII† class in 2D, a novel type of non-Hermitian flux skin effect can emerge, which is different from the $\mathbb{Z}_2$ skin effect discussed above. Moreover, we propose the electric-circuit realization of the topological phase in this class in the SM [46].

For all three spinful classes in 2D, we can use the twisted rectangle with π flux in Fig. 1(c) to construct their topological phases. In such a structure, the mirror symmetry is projectively represented as in Eq. (4). Thus, the gauge-field enriched time-reversal symmetry is

$$\tilde{\mathcal{T}} = \mathcal{M}_z T = i\tau_2 \otimes \sigma_0 K I, \qquad \tilde{\mathcal{T}}^2 = -1, \tag{10}$$

which realizes the required symmetry algebra of Eq. (1).

Our first 2D example is the spinful topological phase in class AII† with only time-reversal symmetry. It possesses the non-Hermitian flux skin effect as its characteristic feature [45,51]. That is, when flux defects are present, extensive numbers of skin modes will be localized at the flux cores. As shown Fig. 3(a1), this model is constructed by the block of Fig. 1(c), which reads,

$$\begin{aligned}
\mathcal{H}_{2D}(k_x, k_y) &= \mathcal{H}(k_x) + \mathcal{H}(k_y), \\
\mathcal{H}(k_y) &= (t_l + t_r)\cos k_y \tau_0 \otimes \sigma_0 + i(t_l - t_r)\sin k_y \tau_3 \otimes \sigma_0, \\
\mathcal{H}(k_x) &= J_R \tau_0 \otimes \sigma_1 + J_I \tau_2 \otimes \sigma_2 + t\cos k_x \tau_0 \otimes \sigma_1 \\
&\quad + t\sin k_x \tau_0 \otimes \sigma_2 + i\gamma \tau_0 \otimes \sigma_1.
\end{aligned} \tag{11}$$

Here, $\mathcal{H}(k_x)$ denotes the Hamiltonian in the x direction, which is composed of the J_R and J_I terms within unit cells, the hopping term t, and the γ term to induce non-Hermiticity. In the y direction, $\mathcal{H}(k_y)$ consists of nonreciprocal hoppings as shown in Fig. 3(a2). The hopping amplitudes are t_r toward right and t_l ($\neq t_r$) toward left on the top layer, while they are exchanged on the bottom layer. The PBC energy spectrum is plotted in Fig. 3(a3).

While $\tilde{\mathcal{T}}$ in Eq. (10) remains to be the time-reversal symmetry for this 2D system, the individual $\mathcal{M}_z$ and T symmetries are broken by the nonreciprocal hoppings in the y direction. Corresponding to $\tilde{\mathcal{T}}$, a $\mathbb{Z}_2$ invariant $\nu_{2D}(E) \in \{0, 1\}$ is defined in Refs. [22,45], where E is a reference energy. We plot $\nu_{2D}(E)$ against E in Fig. 3(a4). The topological invariant takes nontrivial values for E inside the red region, indicating the 2D system is topological.

Different from the 1D case, there is no $\mathbb{Z}_2$ skin effect under full OBC. Instead, a nontrivial magnetic flux response serves as the characteristic feature of this spinful 2D topology [45,51]. By inserting a pair of π flux defects, there will be $\mathcal{O}(L)$ skin modes from the total $\mathcal{O}(L^2)$ modes

localized at the flux cores, where L^2 is the system size. In Fig. 3(a5), the 2D system clearly shows such a non-Hermitian flux skin effect, confirming the nontrivial topology. We provide the calculation details and the finite-size scaling of the flux skin effect in the SM [46].

Our second example is a non-Hermitian generalized spinless Kane-Mele model, which belongs to CII† class in 2D. It is constructed based on the renowned Kane-Mele model, where the spin-orbit coupling is replaced by the spinless block of Fig. 1(c) with adjustments [52], as shown by the next-nearest-neighbor (NNN) hoppings in Fig. 3(b1). These blocks connect the top and bottom layers of the hexagonal lattice. The momentum-space Hamiltonian reads,

$$\mathcal{H}_{\mathrm{KM}}(\boldsymbol{k}) = t\chi_1(\boldsymbol{k})\tau_0 \otimes \sigma_1 + t\chi_2(\boldsymbol{k})\tau_0 \otimes \sigma_2 - 2iJ_R\eta_1(\boldsymbol{k})\tau_0 \otimes \sigma_3 - 2iJ_I\eta_2(\boldsymbol{k})\tau_2 \otimes \sigma_0, \quad (12)$$

where t is the nearest-neighbor hopping amplitude, $\chi_1 + i\chi_2 = 1 + e^{ik_1} + e^{ik_2}$, and $\eta_1 + i\eta_2 = e^{ik_1} + e^{ik_2} + e^{i(k_2-k_1)}$ with $k_{1(2)} = \boldsymbol{k} \times \boldsymbol{b}_{1(2)}$. The primitive vectors are $\boldsymbol{b}_{1(2)} = (3/2, \pm\sqrt{3}/2)$. We plot the PBC spectrum in Fig. 3(b2), which has a point gap with respect to the zero energy.

Besides the time-reversal symmetry of Eq. (10), the system is invariant under the sublattice symmetry $\mathcal{S} = \tau_0 \otimes \sigma_3$ as $\mathcal{S}\mathcal{H}_{\mathrm{KM}}(\boldsymbol{k})^\dagger\mathcal{S}^{-1} = -\mathcal{H}_{\mathrm{KM}}(\boldsymbol{k})$. A 2D topological phase satisfying these symmetries is characterized by a $\mathbb{Z}_2$ Kane-Mele invariant [22]. This invariant can be computed by the extended Hermitian Hamiltonian $\mathcal{H}_H(\boldsymbol{k}) = \mathrm{antidiag}\{\mathcal{H}^\dagger_{\mathrm{KM}}(\boldsymbol{k}), \mathcal{H}_{\mathrm{KM}}(\boldsymbol{k})\}$ [46], where "antidiag" denotes antidiagonal matrices, due to the topological equivalence [21,22,53]. We then calculate the invariant using the Wilson loop spectrum [54]. A nontrivial (trivial) topological invariant corresponds to odd (even) number of crossings of the $\theta = \pi$ reference line. As shown in Fig. 3(b3), this spinful phase possesses a nontrivial $\mathbb{Z}_2$ invariant. More discussions on the topological edge states can be found in the SM [46].

Summary and discussions.—In this Letter, we have presented mechanisms for realizing spinful ramified symmetry classes with the time-reversal symmetry by spinless systems, and systematically constructed experimentally realizable models for all topologically nontrivial cases in one and two dimensions. Our theory may be extended along the two directions, namely all non-Hermitian symmetry classes that contain either original or ramified time-reversal symmetry among the 38-fold symmetry classification, and non-Hermitian systems with other types of energy gaps [42]. This is due to the fact that the essence of our approach relies on the modification of symmetry algebras using gauge fields, which is independent of non-Hermitian ramification and complex-energy gaps. Our Letter shows that ubiquitously existing gauge structures may significantly enrich non-Hermitian physics at the fundamental level, and considering effects of gauge structures would be a promising direction to extend the current framework of non-Hermitian physics.

This work was supported by the Guangdong-Hong Kong Joint Laboratory of Quantum Matter, the NSFC/RGC JRS grant (RGC Grant No. N_HKU774/21, NSFC Grant No. 12161160315), the CRF (Grant No. C6009-20G) and GRF (Grant No. 17310622) of Hong Kong, and the Basic Research Program of Jiangsu Province (Grant No. BK20211506). W. B. R. was supported by the RGC Postdoctoral Fellowship (Ref. No. PDFS2223-7S05).

*wbrui@hku.hk
†yuxinphy@hku.hk
‡zwang@hku.hk

[1] T. E. Lee, Anomalous edge state in a non-Hermitian lattice, Phys. Rev. Lett. **116**, 133903 (2016).
[2] D. Leykam, K. Y. Bliokh, C. Huang, Y. D. Chong, and F. Nori, Edge modes, degeneracies, and topological numbers in non-Hermitian systems, Phys. Rev. Lett. **118**, 040401 (2017).
[3] H. Shen, B. Zhen, and L. Fu, Topological band theory for non-Hermitian Hamiltonians, Phys. Rev. Lett. **120**, 146402 (2018).
[4] H. Zhou, C. Peng, Y. Yoon, C. W. Hsu, K. A. Nelson, L. Fu, J. D. Joannopoulos, M. Soljacic, and B. Zhen, Observation of bulk Fermi arc and polarization half charge from paired exceptional points, Science **359**, 1009 (2018).
[5] F. K. Kunst, E. Edvardsson, J. C. Budich, and E. J. Bergholtz, Biorthogonal bulk-boundary correspondence in non-Hermitian systems, Phys. Rev. Lett. **121**, 026808 (2018).
[6] W. B. Rui, Y. X. Zhao, and A. P. Schnyder, Topology and exceptional points of massive Dirac models with generic non-Hermitian perturbations, Phys. Rev. B **99**, 241110(R) (2019).
[7] C. H. Lee, L. Li, and J. Gong, Hybrid higher-order skin-topological modes in nonreciprocal systems, Phys. Rev. Lett. **123**, 016805 (2019).
[8] F. Song, S. Yao, and Z. Wang, Non-Hermitian topological invariants in real space, Phys. Rev. Lett. **123**, 246801 (2019).
[9] W. B. Rui, M. M. Hirschmann, and A. P. Schnyder, $\mathcal{PT}$-symmetric non-Hermitian Dirac semimetals, Phys. Rev. B **100**, 245116 (2019).
[10] J. Y. Lee, J. Ahn, H. Zhou, and A. Vishwanath, Topological correspondence between Hermitian and non-Hermitian systems: Anomalous dynamics, Phys. Rev. Lett. **123**, 206404 (2019).
[11] T. Yoshida and Y. Hatsugai, Exceptional rings protected by emergent symmetry for mechanical systems, Phys. Rev. B **100**, 054109 (2019).
[12] Y. Ashida, Z. Gong, and M. Ueda, Non-Hermitian physics, Adv. Phys. **69**, 249 (2020).
[13] D. S. Borgnia, A. J. Kruchkov, and R.-J. Slager, Non-Hermitian boundary modes and topology, Phys. Rev. Lett. **124**, 056802 (2020).

[14] L. Li, C. H. Lee, S. Mu, and J. Gong, Critical non-Hermitian skin effect, Nat. Commun. **11**, 5491 (2020).

[15] S. Longhi, Topological phase transition in non-Hermitian quasicrystals, Phys. Rev. Lett. **122**, 237601 (2019).

[16] E. J. Bergholtz, J. C. Budich, and F. K. Kunst, Exceptional topology of non-Hermitian systems, Rev. Mod. Phys. **93**, 015005 (2021).

[17] A. Panigrahi, R. Moessner, and B. Roy, Non-Hermitian dislocation modes: Stability and melting across exceptional points, Phys. Rev. B **106**, L041302 (2022).

[18] W. B. Rui, Y. X. Zhao, and Z. D. Wang, Hermitian topologies originating from non-Hermitian braidings, Phys. Rev. B **108**, 165105 (2023).

[19] P. Delplace, T. Yoshida, and Y. Hatsugai, Symmetry-protected multifold exceptional points and their topological characterization, Phys. Rev. Lett. **127**, 186602 (2021).

[20] W. B. Rui, Z. Zheng, C. Wang, and Z. D. Wang, Non-Hermitian spatial symmetries and their stabilized normal and exceptional topological semimetals, Phys. Rev. Lett. **128**, 226401 (2022).

[21] Z. Gong, Y. Ashida, K. Kawabata, K. Takasan, S. Higashikawa, and M. Ueda, Topological phases of non-Hermitian systems, Phys. Rev. X **8**, 031079 (2018).

[22] K. Kawabata, K. Shiozaki, M. Ueda, and M. Sato, Symmetry and topology in non-Hermitian physics, Phys. Rev. X **9**, 041015 (2019).

[23] S. Yao and Z. Wang, Edge states and topological invariants of non-Hermitian systems, Phys. Rev. Lett. **121**, 086803 (2018).

[24] K. Yokomizo and S. Murakami, Non-Bloch band theory of non-Hermitian systems, Phys. Rev. Lett. **123**, 066404 (2019).

[25] Z. Yang, K. Zhang, C. Fang, and J. Hu, Non-Hermitian bulk-boundary correspondence and auxiliary generalized Brillouin zone theory, Phys. Rev. Lett. **125**, 226402 (2020).

[26] K. Kawabata, N. Okuma, and M. Sato, Non-Bloch band theory of non-Hermitian Hamiltonians in the symplectic class, Phys. Rev. B **101**, 195147 (2020).

[27] M.-A. Miri and A. Alù, Exceptional points in optics and photonics, Science **363**, eaar7709 (2019).

[28] K. Kawabata, T. Bessho, and M. Sato, Classification of exceptional points and non-Hermitian topological semimetals, Phys. Rev. Lett. **123**, 066405 (2019).

[29] T. Kato, *Perturbation Theory for Linear Operators*, 2nd ed., Classics in Mathematics (Springer-Verlag, Berlin Heidelberg, 1995), 10.1007/978-3-642-66282-9.

[30] W. D. Heiss, The physics of exceptional points, J. Phys. A **45**, 444016 (2012).

[31] M. Berry, Physics of Nonhermitian Degeneracies, Czech. J. Phys. **54**, 1039 (2004).

[32] Y. Xu, S.-T. Wang, and L.-M. Duan, Weyl exceptional rings in a three-dimensional dissipative cold atomic gas, Phys. Rev. Lett. **118**, 045701 (2017).

[33] N. Okuma, K. Kawabata, K. Shiozaki, and M. Sato, Topological origin of non-Hermitian skin effects, Phys. Rev. Lett. **124**, 086801 (2020).

[34] K. Zhang, Z. Yang, and C. Fang, Correspondence between winding numbers and skin modes in non-Hermitian systems, Phys. Rev. Lett. **125**, 126402 (2020).

[35] T. Helbig, T. Hofmann, S. Imhof, M. Abdelghany, T. Kiessling, L. W. Molenkamp, C. H. Lee, A. Szameit, M. Greiter, and R. Thomale, Generalized bulk–boundary correspondence in non-Hermitian topolectrical circuits, Nat. Phys. **16**, 747 (2020).

[36] A. Ghatak, M. Brandenbourger, J. van Wezel, and C. Coulais, Observation of non-Hermitian topology and its bulk–edge correspondence in an active mechanical metamaterial, Proc. Natl. Acad. Sci. U.S.A. **117**, 29561 (2020).

[37] K. Zhang, Z. Yang, and C. Fang, Universal non-Hermitian skin effect in two and higher dimensions, Nat. Commun. **13**, 2496 (2022).

[38] H. Zhou and J. Y. Lee, Periodic table for topological bands with non-Hermitian symmetries, Phys. Rev. B **99**, 235112 (2019).

[39] D. Bernard and A. LeClair, *A Classification of Non-Hermitian Random Matrices* (Springer, Dordrecht, 2002), 10.1007/978-94-010-0514-2_19.

[40] S. Lieu, Topological symmetry classes for non-Hermitian models and connections to the bosonic Bogoliubov–de Gennes equation, Phys. Rev. B **98**, 115135 (2018).

[41] Note that the $\mathrm{AZ}^\dagger$ classification is also tenfold, same as AZ classification. But because two of $\mathrm{AZ}^\dagger$ classes (A, AIII) are identical to those in AZ classes, the number of additional ramified symmetry classes is eight. Among the eight ramified $\mathrm{AZ}^\dagger$ classes, six of them are independent and are not equivalent to those in AZ classes [22].

[42] There are two types of non-Hermitian energy gaps: one is point gap and the other is line gap [22]. For a non-Hermitian Hamiltonian $H(\boldsymbol{k})$ to have a point gap with respect to a energy point E_P, it is invertible about E_P ($\det|H(\boldsymbol{k}) - E_P| \neq 0$) and all the eigenenergies are not equal to E_P.

[43] The usual convention for the eight real Altland-Zirnbauer symmetry classes is to specify $T^2 = \eta_T = \pm 1$ and $C^2 = \eta_C = \pm 1$. Our convention is to specify $T^2 = \eta_T$ and $TS = \alpha_S ST$ with $\alpha_S = \pm 1$, because sublattice symmetry S is natural for nonsuperconducting systems. One may use $C = ST$ to translate the two conventions into each other.

[44] Y. Yi and Z. Yang, Non-Hermitian skin modes induced by on-site dissipations and chiral tunneling effect, Phys. Rev. Lett. **125**, 186802 (2020).

[45] N. Okuma and M. Sato, Non-Hermitian topological phenomena: A review, Annu. Rev. Condens. Matter Phys. **14**, 83 (2023).

[46] See Supplemental Material at http://link.aps.org/supplemental/10.1103/PhysRevLett.131.176402 for the representative models in the rest nontrivial spinful symmetry classes, the electric-circuit realization in experiments, and other calculation details, which includes Refs. [22,35,47–49].

[47] S. Weidemann, M. Kremer, T. Helbig, T. Hofmann, A. Stegmaier, M. Greiter, R. Thomale, and A. Szameit, Topological funneling of light, Science **368**, 311 (2020).

[48] L. Zhang, Y. Yang, Y. Ge, Y.-J. Guan, Q. Chen, Q. Yan, F. Chen, R. Xi, Y. Li, D. Jia, S.-Q. Yuan, H.-X. Sun, H. Chen, and B. Zhang, Acoustic non-Hermitian skin effect from twisted winding topology, Nat. Commun. **12**, 6297 (2021).

[49] D. Nakamura, T. Bessho, and M. Sato, Bulk-boundary correspondence in point-gap topological phases, arXiv:2205.15635.

[50] M. Nakahara, *Geometry, Topology and Physics* (CRC Press, Boca Raton, 2018).

[51] M. M. Denner and F. Schindler, Magnetic flux response of non-Hermitian topological phases, SciPost Phys. **14**, 107 (2023).

[52] We note that the adjustments in the Fig. 3(b1) right panel, i.e., NNN hoppings, do not break the $\tilde{\mathcal{T}}$ symmetry in Eq. (10), and they turn the system to non-Hermitian. This is because for the NNN hoppings between A sublattices, we simply multiply a $-i$ coefficient to the original block of Fig. 1(c); for the NNN hoppings between B sublattices, it is obtained by exchanging the two middle sticks (hoppings) between the top and bottom row of Fig. 1(c), and then multiplying by i, which does not change the mirror-reflection symmetry $\mathcal{M}_z$.

[53] R. Roy and F. Harper, Periodic table for floquet topological insulators, Phys. Rev. B **96**, 155118 (2017).

[54] R. Yu, X. L. Qi, A. Bernevig, Z. Fang, and X. Dai, Equivalent expression of $\mathbb{Z}_2$ topological invariant for band insulators using the non-Abelian berry connection, Phys. Rev. B **84**, 075119 (2011).